ARTICLE NO. 80-4030

C80-039

00001
20007
20019

Flight Measurements of a Wing Tip Vortex

Ronald L. Panton,* William L. Oberkampf,† and Nicola Soskic‡
The University of Texas, Austin, Texas

Detailed flight measurements of the wing tip vortex generated by a DeHavilland Beaver were made with instruments mounted on a sailplane, which was towed behind the aircraft. Data at three different downstream locations were obtained by using three different tow rope lengths. The measurement stations were 4, 8, and 16 span lengths behind the aircraft, and the vortex Reynolds number was slightly above $\Gamma_0/\nu = 10^6$. Results of the tests differed considerably from those of previous authors. Although the customary similarity variables for vortex decay were verified, the velocities were a factor of 2.5 higher than previous results. The vortex core radius and turbulence levels also proved to be substantially smaller than earlier measurments. These results indicate that the final similarity state of the vortex may depend strongly upon the initial tip shape, initial turbulence levels of the vortex, and/or the ambient turbulence levels.

Nomenclature

a	= Squire's constant ($\nu_t = a\Gamma_0$)
AR	= aspect ratio
b	= span
c (or C)	= chord
C_L	= lift coefficient
k_1, k_2, k_3	= constants in Eq. (2)
r (or R)	= radial distance from vortex core
r_1	= radius at which maximum tangential velocity occurs
r_*	= nondimensional radial distance
T_∞	= freestream temperature
V_∞	= freestream velocity
V_θ	= vortex tangential velocity
$V_{\theta 1}$	= maximum vortex tangential velocity
V_θ^*	= nondimensional tangential velocity, Eq. (3)
V_r	= radial velocity
W	= aircraft weight
x	= downstream distance from wing tip
x_0	= effective origin of vortex
x_i	= position coordinate in plane of probes
x_v	= position of vortex center in plane of probes
y_i	= position coordinate in plane of probes
y_v	= position of vortex center in plane of probes
α	= angle of attack
γ_j	= angle between perpendiculars giving vortex estimate j
Γ_0	= circulation constant for vortex
Γ_{0w}	= circulation constant for wing
ρ_∞	= freestream density
ν	= molecular kinematic viscosity
ν_t	= turbulent viscosity constant in Eq. (1)

Introduction

CURRENT knowledge of the decay of a turbulent wing tip vortex divides the process into two stages. The first stage, identified by the experiments of Ciffone and Orloff,[1] is a plateau region where the maximum velocity only slightly decays. Iversen[2] interprets this region as an adjustment phase where more highly damped components in the initial profile die out, leaving the turbulent Lamb vortex as the fundamental similarity component. The mathematics of this description are the same as the mathematics of the decay of a laminar vortex with an arbitrary initial profile (de Neufville[3]).

Following the plateau region is the so-called similarity region, where the maximum velocity decays as $x^{-1/2}$, while the core radius grows as $x^{+1/2}$. One of the first theoretical contributions to this problem was made by Squire,[4] who proposed that a constant eddy viscosity could be used in the decay equation for Lamb's laminar vortex. He also proposed that the viscosity would be proportional to the strength of the vortex $\nu_t = a\Gamma_0$. This implies that the ratio of $\nu_t/\nu = a\Gamma_0/\nu$ would increase indefinitely with the vortex Reynolds number Γ_0/ν. Under these conditions a single similarity solution exists, which is independent of the Reynolds number Γ_0/ν. By correlating a considerable amount of experimental data, Iversen[5] found that Squire's assumption was valid above a Reynolds number of $\Gamma_0/\nu = 10^6$, and that in this regime turbulence dominates the vortex. There are many other theoretical computations of vortex decay having various degrees of complexity. One of the latest and most complex is that of Knight and Saffman.[6] This theory is notable in that it produces a similarity state which is strongly dependent upon Γ_0/ν and has a core without turbulence.

Measurements on wing tip vortices and their far field behavior are, at best, a difficult task. Flight tests, where the Reynolds numbers are high, are usually limited in both the quantity and quality of information that can be obtained. The object of this research program was to take many detailed velocity measurements and, at the same time, maintain the vortex Reynolds number above 10^6. The experiments were conducted using a DeHavilland Beaver aircraft to generate the vortex. The Beaver also towed a sailplane, which carried an instrument platform containing an array of hot-film anemometers. The pilot of the sailplane could maneuver the instruments into the vortex, so that detailed velocity profiles could be obtained. By changing the tow rope length on different flights, it was possible to make measurements at three downstream locations of 4, 9, and 18 span lengths. These locations turned out to be in the similarity decay region.

The results of our measurements do not correlate with previous experimental measurements. Although the $x^{-1/2}$ decay was observed, the magnitude of the tangential velocity was much larger than others report. Coinciding with this, we found that the turbulent intensities and eddy viscosity were substantially below previous results.

Received April 17, 1979; revision received Nov. 1, 1979. This paper is declared a work of the U.S. Government and therefore is in the public domain. Reprints of this article may be ordered from AIAA Special Publications, 1290 Avenue of the Americas, New York, N.Y. 10019. Order by Article No. at top of page. Member price $2.00 each, nonmember, $3.00 each. **Remittance must accompany order.**

Index categories: Aerodynamics; Jets, Wakes and Viscid-Inviscid Flow Interactions; Viscous Nonboundary-Layer Flows.

*Professor, Mechanical Engineering Dept. Associate Fellow AIAA.

†Associate Professor, Mechanical Engineering Dept. Member AIAA.

‡Graduate Research Assistant, Mechanical Engineering Dept. Presently at the University of Sarajevo, Sarajevo, Yugoslavia.

Fig. 1 DeHavilland Beaver aircraft.

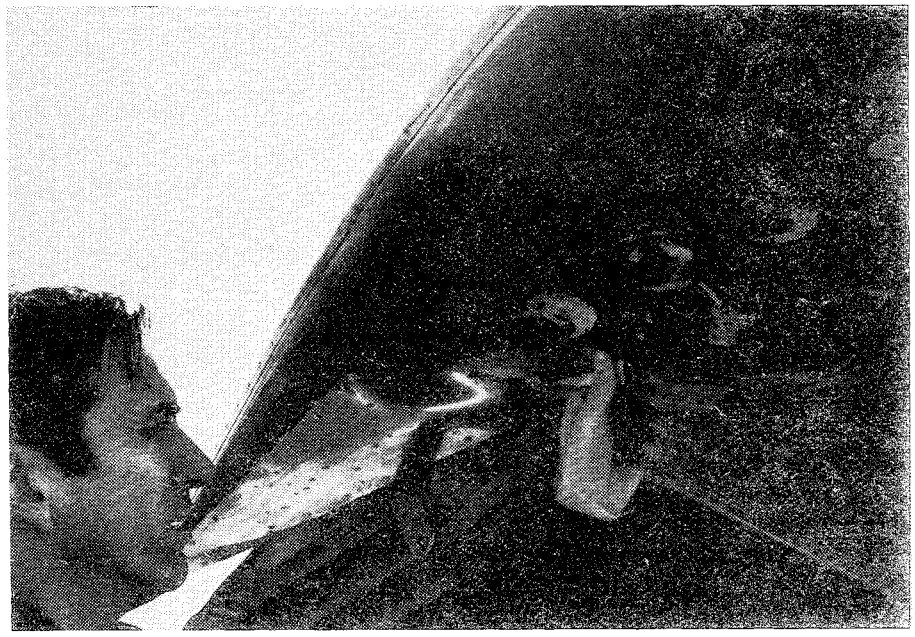

Fig. 2 Wing tip and flare installation.

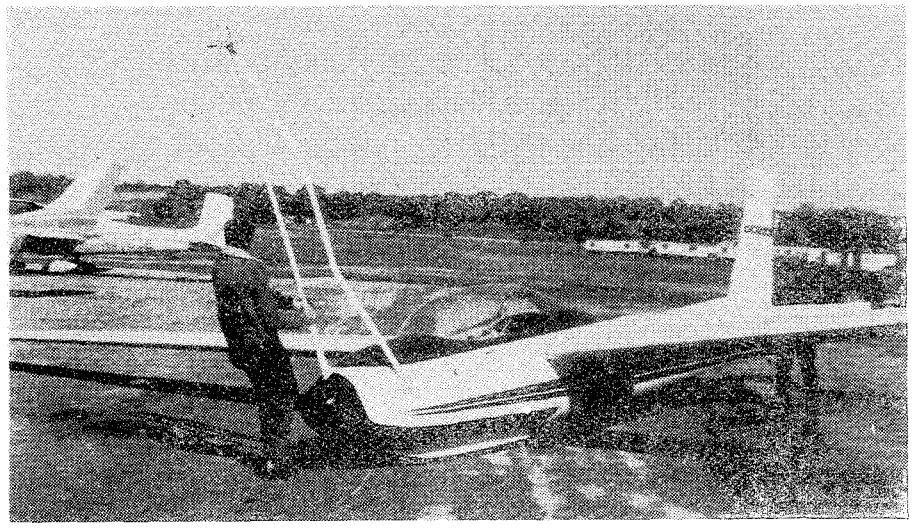

Fig. 3 Schweizer 2-32 sailplane.

Test Equipment and Procedures

The DeHavilland Beaver aircraft (Fig. 1) which generated the vortex is a single-engine monoplane with a textbook wing. The wing is straight, untwisted, and has a constant chord. A simple tip fairing as shown in Fig. 2 terminated the section. Specifications of the airplane and the sailplane are given in Table 1.

In order for the sailplane pilot to locate the vortex it was necessary to mark the vortex with smoke. This was accomplished using smoke flares which were mounted in canisters and recessed into the Beaver wing tip. A single flare would last 1-2 minutes after being started by an electric ignitor. A tortuous flow path through the canister caused a large part of the smoke to condense within the canister. This was done purposely in order to minimize the amount of smoke and avoid contamination of the hot-film elements. Contamination of the hot films did not occur, as repeated calibration of the hot films throughout the program showed no significant changes.

Table 1 Aircraft specifications

	DeHavilland Beaver DHC-2	Schweizer 2-32
Wing span, m (ft)	14.6 (48.0)	17.4 (57.1)
Wing chord, m (ft)	1.59 (5.21) (constant)	1.45 (4.75) (root)
Aspect ratio	9.2	18.05
Wing area, m^2 (ft^2)	23.2 (250)	16.7 (180)
Length, m (ft)	9.24 (30.33)	8.15 (26.75)
Weight (empty), kg (lbm)	1361 (3000)	385 (850)
Weight (maximum), kg (lbm)	2313 (5100)	608 (1340)
Stall speed, m/s (mph)	26.8 (60)	21.5 (48)

Figure 3 shows the Schweizer 2-32 sailplane and the tower upon which the hot-film sensors were mounted. The extreme height of the tower (2.75 m) was required so that the vortex would not interact with the sailplane rudder during the measurements. This height also assured minimum interference between the sailplane flowfield and the vortex. Mounted on top of the tower were three hot-film probes (Thermo Systems Inc., model 1294), each containing three sensor elements. These probes measured all three velocity components. In addition to recording the full signal from all sensors, turbulence measurements were recorded by ac coupling and further amplifying the signals from one probe. The measurement system was completed by several other instruments to determine the flight conditions. A pitot-static probe mounted on the tower was connected to a pressure transducer so that an indication of air speed could be recorded. Likewise, a static pressure, referenced to a thermos bottle, and a thermister gave information on altitude and temperature.

All signals were recorded on a 14-channel tape recorder which was carried in the sailplane and controlled by the pilot. The tape recorder met IRIG intermediate-band specifications at the operating speed of 30 ips. The nine dc hot-film signals, three ac hot-film signals, and a timing channel occupied 13 channels. All the slowly changing parameters, pressure and temperature, were multiplexed onto the last channel. Comments from the glider pilot were also recorded on an edge track.

Flights were accomplished during the early morning hours when the air was calm and stable. Testing was not feasible during the summer months, because the ambient turbulence was always too high. It turned out that all the data reported herein were taken in an air mass of northern origin. A typical flight procedure was to monitor the temperature as the glider and tow plane climbed. Once above the convective layer, another 600 m (2000 ft) of altitude was gained before making a measurement run. Test altitudes varied from 1200 to 2200 m (4000-7200 ft). Before and after each smoke flare, a hot-film probe calibration run was made with the glider flying directly behind the tow plane in the high-tow position. After a calibration run, the sailplane would take a position behind and below the wing tip of the tow plane. Once the smoke flare was ignited and the sailplane pilot could see the vortex core, he would position the instrument tower directly below the vortex. It was necessary for the pilot to concentrate on the tow plane wing tip and use peripheral vision to observe the vortex. When the sailplane was aligned laterally with the vortex, the pilot would gradually allow the sailplane to rise so the probes passed through the vortex. Shortly after the probes passed above the vortex core, the vortex interacted with the rudder and caused a significant yaw disturbance on the sailplane. Several passes through the vortex could be made on the same smoke flare.

The flight characteristics of the tow plane and sailplane dictated that the testing be done at 40 m/s air speed (88 mph). Below this speed the tow plane lost its damping in yaw, while at higher speeds the glider wings produced so much lift that it was hard to keep the glider from climbing. After all flares had been used, the sailplane would release the tow rope and perform a series of calibration runs at different speeds. These runs allowed a check on the laboratory calibration of the hot-film probes and verified that the calibration was not drifting because of contamination.

Data Reduction Procedures

The large amount of data obtained made it necessary to automate the calculation procedures on a computer. Tape

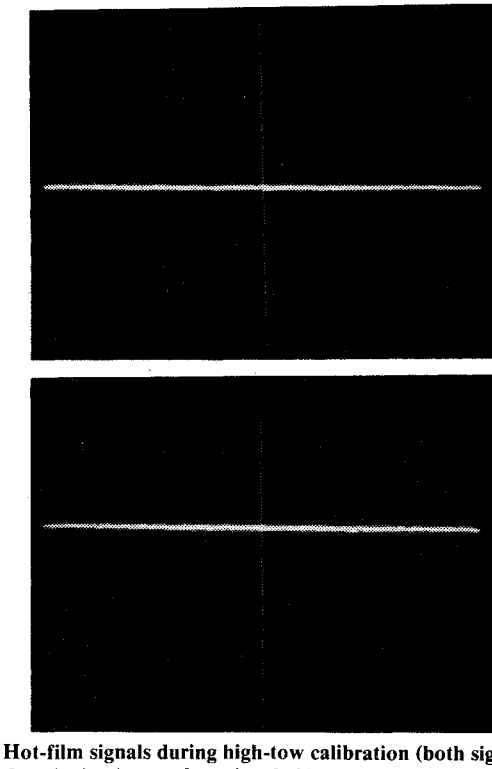

Fig. 4 Hot-film signals during high-tow calibration (both signals are 10 s in duration): a) complete signal, b) ac coupled and amplified signal.

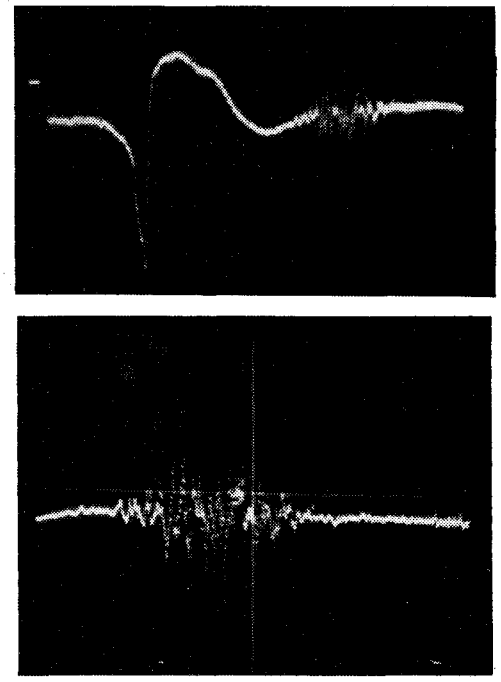

Fig. 5 Typical hot-film signals during pass through vortex: a) full signal of 10 s duration, b) ac turbulence signal of 5 s duration.

Table 2 Individual probe velocities measured during high tow calibration

Flight No.	Flare No.	Probe 1 Velocity, m/s	Probe 1 Angle, deg	Probe 2 Velocity, m/s	Probe 2 Angle, deg	Probe 3 Velocity, m/s	Probe 3 Angle, deg
18	1	40.9	6.7	40.2	3.8	39.8	5.3
12	1	38.8	6.3	37.8	3.3	37.8	5.2
12	2	40.4	7.2	39.4	4.0	39.3	6.8
12	3	39.8	2.4	39.1	2.4	38.7	0.9
15	1	43.0	4.1	42.6	2.0	41.7	2.1
15	2	40.3	8.0	39.4	4.4	39.1	6.4
15	3	41.7	2.8	41.2	1.9	40.5	0.7

Table 3 Measurement conditions

x,m	x/b	V_∞,m/s	T_∞,°C	ρ_∞, kg/m^3	W,kg	Γ_{0w}, m^2/s	C_L	α, deg
62.8	4.29	42.25	10.6	0.935	1720	32.1	0.87	7.2
128	8.75	38.62	8.3	1.097	1630	28.4	0.84	7.0
259	17.7	40.17	10.0	0.984	1710	31.9	0.91	7.7

recordings from a flight were first digitized (100 samples/s) to produce digital tapes suitable for the computer. Strip chart records of the flight tapes were also made, so that the sections where the probes passed through the vortex could be identified for further processing. Figure 4 shows a hot-film signal of 10 s duration taken during a high-tow calibration run. Both the dc and the amplified ac signals clearly show how smooth and stable the flight conditions were. During a pass through the vortex the signals typically look like those given in Fig. 5.

The high-tow calibration runs gave an opportunity to compare the hot-film probes with each other and to make a correction for mounting misalignment and calibration errors. This was done by adding voltage corrections to each sensor, so that each probe would give the same sailplane velocity (both magnitude and direction). The amount of the correction was never greater than a few percent, as can be seen by comparing the uncorrected values given in Table 2.

By far the most complicated data reduction task was finding the velocity components in a cylindrical coordinate system on the vortex. The basic assumption in locating the vortex core was that the plane defined by the sensing points of the three probes was perpendicular to the axis of a symmetric vortex. The velocity components in this plane (Fig. 6) are then the tangential velocity components of the vortex. A line perpendicular to the tangential velocity should pass directly through the center of the vortex. Since there were three probes, three estimates of the vortex center location were obtained. When the lines from two probes intersect at a small angle, this system of locating the vortex center becomes inaccurate. This problem was accounted for by averaging the intersections (x_j,y_j) as weighted by the $\sin^2$ of the intersection angle. The vortex core location was then detemined by the equations

$$x_v = \sum_{j=1}^{3} \frac{\sin^2\gamma_j}{\Delta} x_j$$

$$y_v = \sum_{j=1}^{3} \frac{\sin^2\gamma_j}{\Delta} y_j$$

where

$$\Delta = \sum_{j=1}^{3} \sin^2\gamma_j$$

This process of locating the vortex center worked well except for two instances: when the vortex was far away from the probes, and when the center of the vortex was very near one of the probes. For example, in the second case, the probe might lie within the triangle formed by the three original intersections. A special method to handle this situation was devised. It essentially minimized the radial velocity of the probe closest to the vortex center. The details of this procedure are given in Ref. 7.

One of the major goals at the outset of the program was to measure the turbulence properties of the vortex. After a series of preliminary flights it became obvious that the turbulence level was so low that it was necessary to ac couple the sensors and provide extra amplification before the signals would be large enough to record. The turbulence signals were digitized at a sample rate of 20,000 Hz which produced 200 turbulence samples for each mean flow sample. The vortex position used to decompose the turbulence components was a running average among the five mean flow values centered about the turbulence data block.

Results

Results from measurements made at three different x distances behind the tow plane will be presented. A complete summary of flight conditions is given in Table 3. In this table the estimates of the angle of attack α, the lift coefficient C_L, and the root circulation Γ_{0w} were made from the manufacturers' data together with the measured freestream conditions and a calculated aircraft weight W. Our tests are at moderate distances behind the aircraft, 4-18 span lengths, and at a fairly

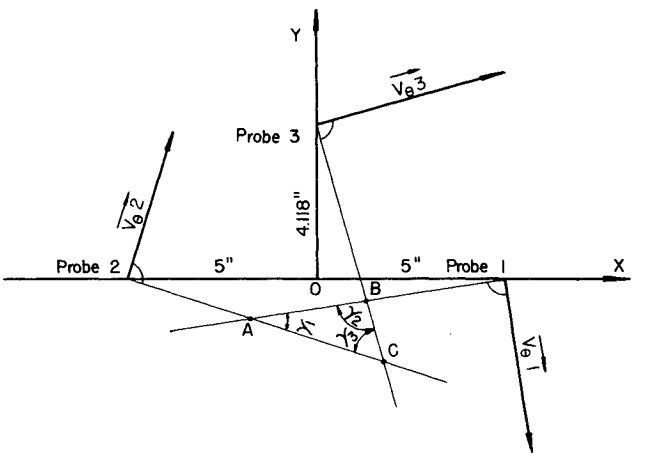

Fig. 6 Vortex center location and velocity decomposition in plane perpendicular to vortex.

high vortex Reynolds number of $\Gamma_0/\nu \approx 10^6$. This Reynolds number is based upon the vortex circulation and not the root circulation Γ_{0w}.

Three flights were selected for detailed analysis. Unfortunately, there was an instrumentation failure after the first flare for the shortest rope length. Nevertheless, there were five good passes through the vortex on this flare giving sufficient data to report. The flights with the two longer rope lengths contained three good flares each and yielded 18 and 11 good passes, respectively, through the vortex.

Of primary interest are the profiles of tangential velocity shown in Figs. 7-9. Considerable scatter in the tangential velocity data seems to be due to the inaccurate location of the vortex center. Another explanation could be that the assumption of a symmetric vortex is inaccurate. These problems were overcome by processing a very large number of measurements. A least-squares method was used to fit the data to the Lamb vortex equation with constant eddy diffusivity (as proposed by Squire[4]). The equation is

$$\frac{V_\theta}{V_\infty} = \frac{\Gamma_0}{2\pi V_\infty C}\,\frac{c}{r}\cdot\left\{1-\exp\left[-\left(\frac{r}{c}\right)^2\cdot\frac{c^2 V_\infty}{4(x-x_0)\nu_t}\right]\right\} \quad (1)$$

The fit at each x position yields values of Γ_0 and the combination $(x-x_0)\nu_t$. Many investigators[5,6,8-11] have made more sophisticated predictions of vortex velocity profiles which show significant deviations from Squire's model. For this reason, a second model equation, where the diffusivity was allowed to be a function of radius, was also tried. It contained three coefficients, two more than the previous equation, and had the following form:

$$\frac{4(x-x_0)\nu_t}{c^2 V_\infty} = k_1 + k_2\left(\frac{r}{c}\right)^2\exp\left[-k_3\left(\frac{r}{c}\right)^2\right] \quad (2)$$

The greater flexibility of this equation produced curves with the peak velocity at a smaller radius; however, outside the core both equations gave the same result. As can be seen in Figs. 7-9, there are actually very few data points within the core; therefore, we concluded that the extra constants in Eq. (2) could not be justified on the basis of the present measurements. The curve outside the peak velocity is well represented by the Lamb vortex, and we proceeded to use this equation in a subsequent similarity analysis. Deviations from the Lamb vortex may occur near the peak and within the core, but our data are not dense enough in these regions to pick out the curve with any confidence.

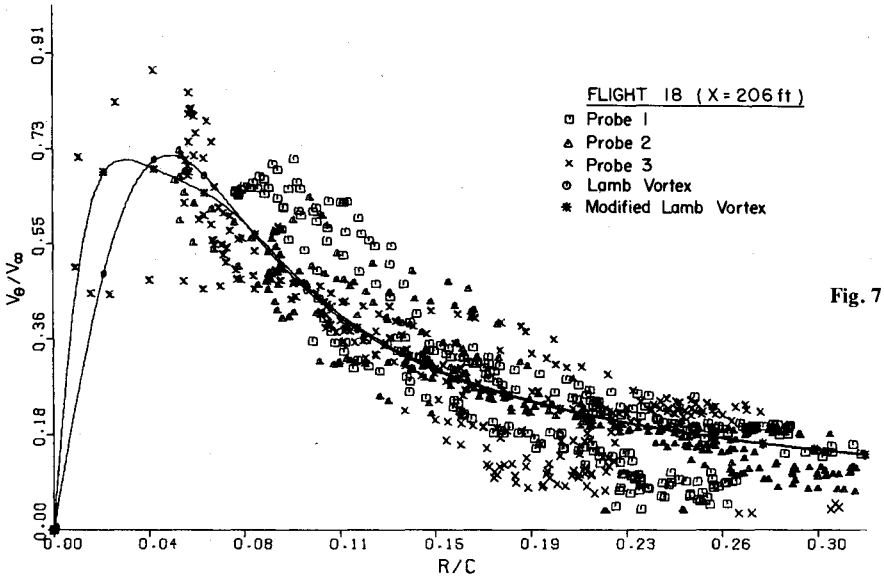

Fig. 7 Tangential velocity at 63 m (206 ft) behind wing.

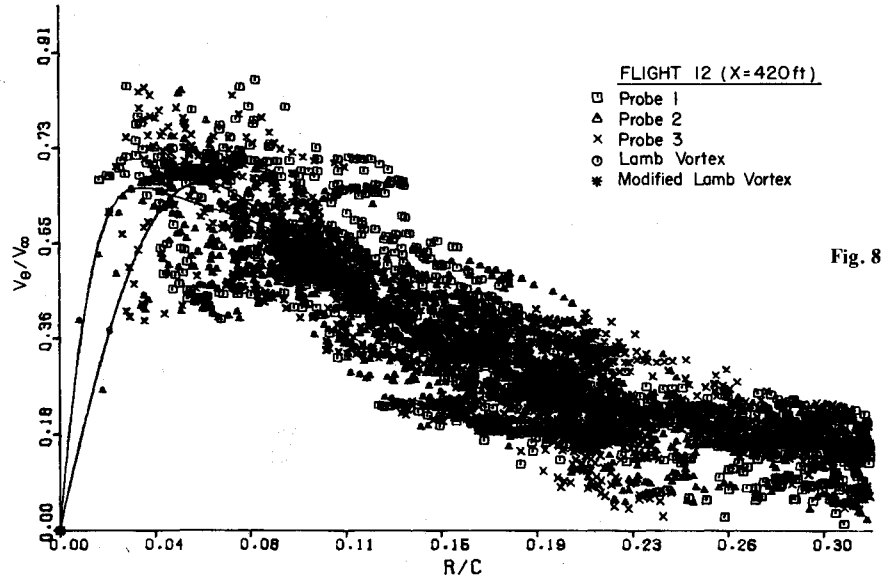

Fig. 8 Tangential velocity at 122 m (402 ft) behind wing.

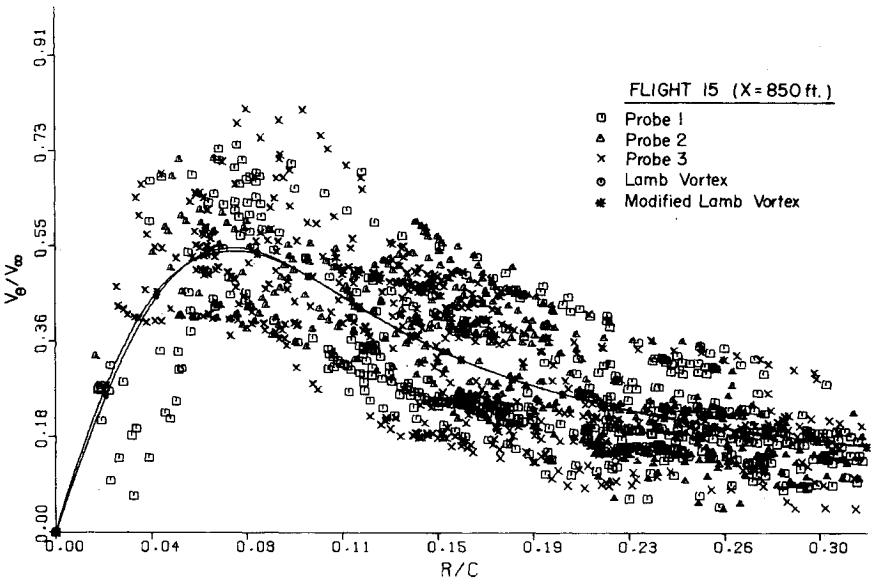

Fig. 9 Tangential velocity at 259 m (850 ft) behind wing.

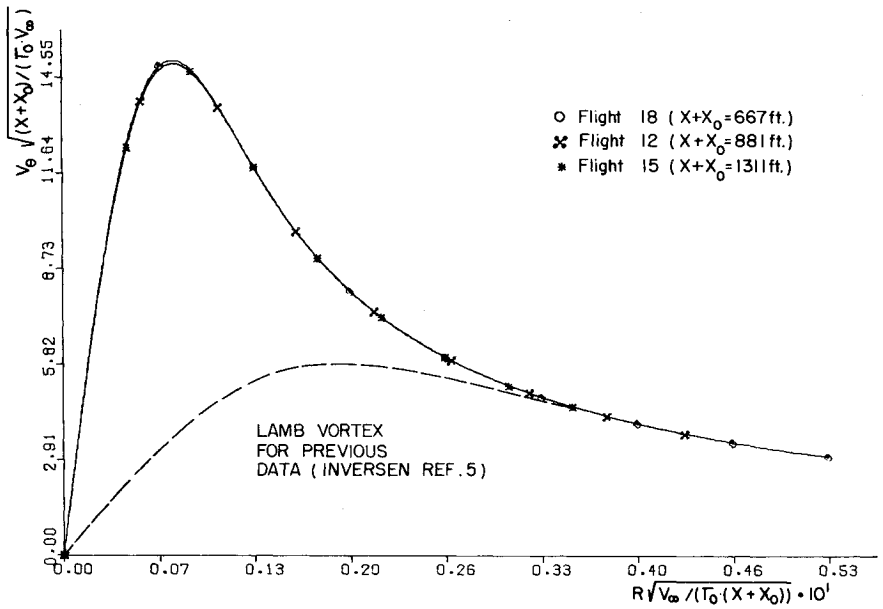

Fig. 10 Tangential velocity in similarity variables.

Table 4 Vortex characteristics

x, m	$\frac{x-x_0}{b}$	Γ_0, m²/s	Γ_0/ν	Γ_0/Γ_{0w}	r_1/c	$V_{\theta 1}/V_\infty$	$\frac{(x-x_0)\Gamma_0 AR^2}{V_\infty b^2}$	$\frac{V_{\theta_1} b}{\Gamma_0 AR}$
62.8	13.9	19.3	$1.02\cdot10^6$	0.60	0.046	0.72	36.9	2.48
128	18.4	20.3	$1.25\cdot10^6$	0.71	0.057	0.66	55.9	2.01
259	27.3	21.1	$1.16\cdot10^6$	0.66	0.069	0.54	83.3	1.64

The most striking feature of the curves is the large value of the maximum $V_{\theta 1}$; it is 72% of the freestream velocity for the shortest rope position. Values of this magnitude have been reported in wind tunnel tests for very high angles of attack, but our angles are much below these values. Later it is shown that the measured V_θ distribution is also higher than previous experiments when expressed in similarity form. It is important to note that the vortex location error discussed earlier causes the maximum tangential velocity measurements to appear lower, not larger. A summary of the vortex characteristics is given in Table 4. It is also of interest to note that the circulation constant for the vortex Γ_0 is 60-70% of the wing root circulation calculated from the aircraft weight. The circulation constant is influenced by the span loading, however, 0.6-0.7 is also a high value compared to previous measurements on rectangular wings.

If the similarity assumption is made for two downstream positions, then the virtual origin of the vortex x_0 and the turbulent diffusivity $\nu_t/\Gamma_0 \equiv a$ (also called Squire's constant) can be calculated. In similarity form (i.e., ν_t is the same constant for all profiles) Eq. (1) becomes

$$V_\theta^* = \frac{1}{2\pi r^*}\left[1-\exp\left(-r^{*2}/4\nu_t/\Gamma_0\right)\right] \tag{3}$$

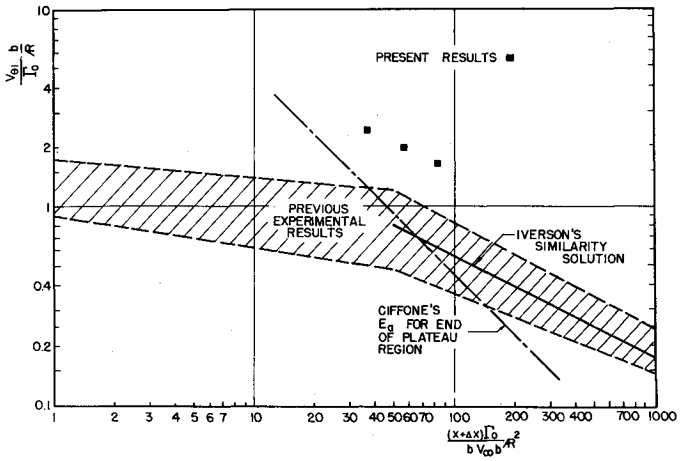

Fig. 11 Decay of maximum tangential velocity with axial distance.

where

$$V_\theta^* = \frac{V_\theta}{\sqrt{\Gamma_0 V_\infty/(x-x_0)}}$$

$$r^* = \frac{r}{\sqrt{\Gamma_0 (x-x_0)/V_\infty}}$$

With the assumption that similarity existed for the two longest rope lenghts, x_0 was determined to be 140 m (461 ft) in front of the wing, and Squire's constant was $\nu_t/\Gamma_0 = 1.1\times10^{-5}$. This gives a ratio of turbulent to molecular diffusivity of only $\nu_t/\nu = 12.5$.

Although Iversen used virtual origins in correlating data from a wide variety of experiments, he did not tabulate the distance from the virtual origin to the wing tip. Presumably this distance depends upon the near field rollup events and may be influenced by the tip shape as well as the spanwise lift distribution. Our value of Squire's constant is quite low compared to previous investigators (cf. Iversen,[5] Fig. 11). Such a low value is the direct result of our high values of vortex tangential velocity.

The fact that similarity exists between all three profiles is confirmed in Fig. 10. On this figure, the constants determined from the two downstream positions are used to nondimensionalize the data from the shortest rope position. All three profiles collapse onto a single curve with an accuracy which is much greater than one would expect. In order to compare with previous results, we have plotted the curve for a Lamb vortex using the constant eddy viscosity value found by Iversen[5] ($\nu_t/\Gamma_0 = 7.66\times10^{-5}$). This curve represents the Lamb vortex having the same maximum velocity as the experiments (at high *Re*) which Iversen correlated. The maximum normalized tangential velocity of our experiments is 15 compared to 5.8 as an average for previous experiments.

Note that this difference must be explained on the basis of a low value of the ratio of ν_t to Γ_0. A high value of Γ_0 compared to the root circulation (Γ_{0w}) means nothing to the vortex. The lift distribution determines the ratio Γ_0/Γ_{0w}. The circulation constant Γ_0 measures the amount of vorticity within the vortex (by Stokes' theorem). According to complete similarity theory, ν_t/Γ_0 should take on a unique distribution determined solely by the local flow situation. The initial velocity profile and initial turbulence level should be completely forgotten. One interpretation of our results is that the initial situation is remembered through a decreased value of the ratio ν_t/Γ_0.

Another comparison with pervious results is given in Fig. 11, where the maximum tangential velocity is plotted as a function of downstream distance. This figure has been adapted from Iversen and displays the plateau region up to a nondimensional distance of about 50, where the similarity region begins. Our experiments are significantly higher, with two points definitely in the similarity region. Although Iversen found that the plateau region ended at 50, Ciffone,[12] on the basis of tow tank experiments, proposed that the end of the plateau region depends upon the initial strength of the vortex. Ciffone's proposed equation is plotted on Fig. 11 and shows that all of our data should be in the similarity region.

The Betz model of the vortex wake structure is an inviscid, small perturbation theory. Although the assumptions required by the theory break down at the tip, the theory can still be used to gain an insight into the vortex flow. Results from the Betz theory can be expressed in the form

$$\frac{V_\theta}{V_\infty} = \frac{\Gamma_{0w}}{cV_\infty} \cdot F\left(\frac{r}{c}; \text{span loading}\right) \tag{4}$$

In this equation Γ_{0w} is the root circulation and conceptually different from the constant Γ_0 in Eq. (1). A comparsion of the Betz theory calculation and the measurements is made in Fig. 12. At large r/c the theory and measurements agree, but the Betz model does not produce the proper middle and inner

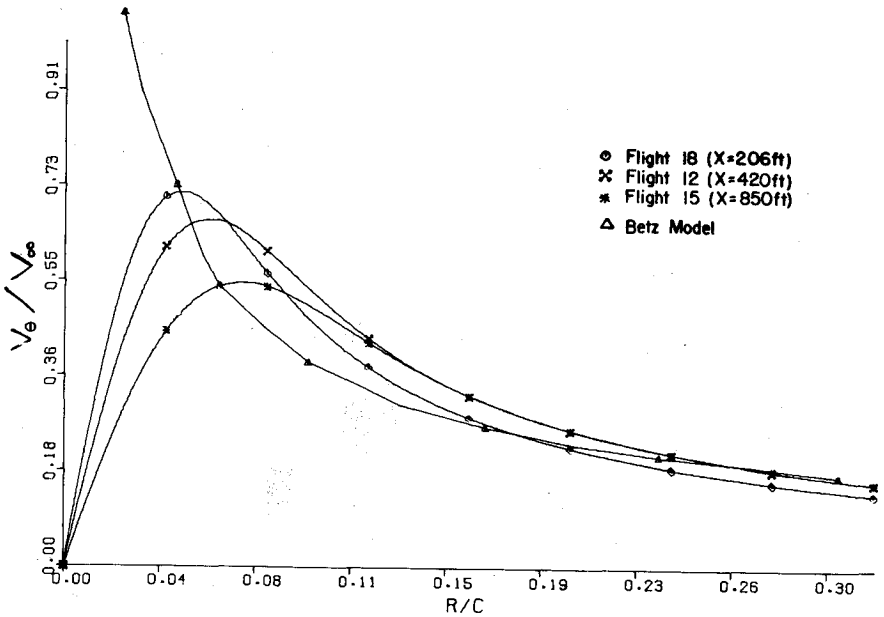

Fig. 12 Betz inviscid theory compared to measurements.

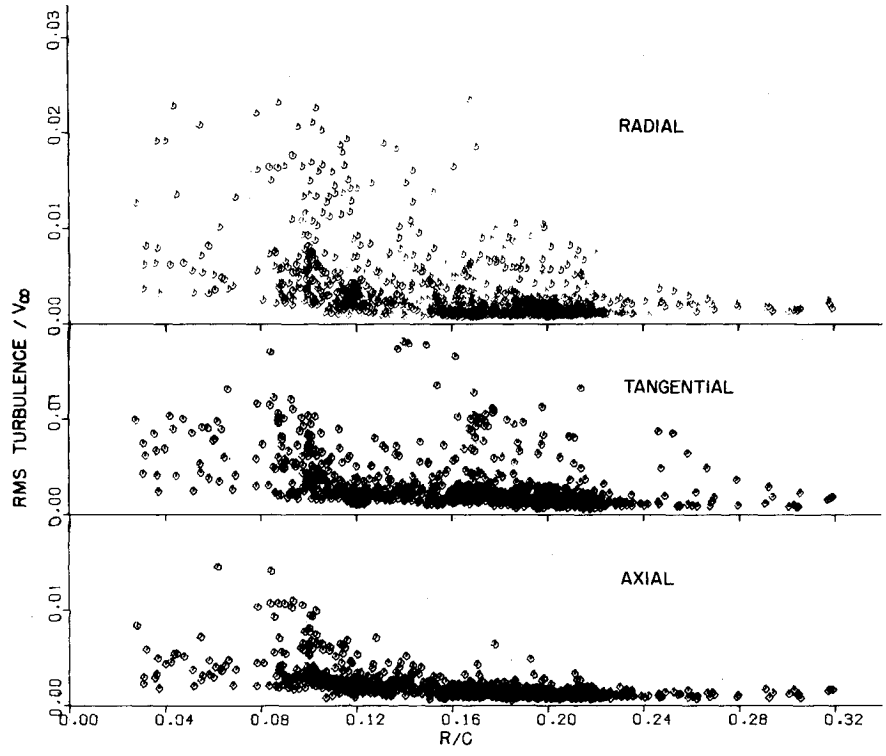

Fig. 13 Turbulence rms intensities normalized by freestream velocity.

portions of the vortex. These portions of the curve depend critically upon the lift distribution near the tip, the region where perturbation theory and the inviscid assumption are not valid.

Radial and axial velocity profiles were also derived from the data and are available in Ref. 7. The radial velocity profiles showed a scatter about zero of $\pm 0.1 V_r/V_\infty$. This is slightly less than half the scatter observed in the tangential velocity profiles. The axial velocities had slightly more scatter than the radial velocities without any discernable trends. It is well known that axial flow in the core region exists, that it changes directions as the angle of attack is changed,[13] and that it is strongly affected by the tip shape.[14] It was a coincidence that our angle of attack was near the region where the reversal in axial flow direction occurs.

The turbulence level in the vortex was much lower than anticipated. Figure 13 displays the rms intensities for each component as a function of radial position. As the core is approached, there is a slight tendency for the level to increase, but the majority of points are always below 0.5% turbulence. This is true even for the points within the core, although there are not as many in that region. In contrast to our results, Singh and Uberoi[15] report 4% turbulence levels ($x/c=80$, $\Gamma_0/\nu \approx 10^5$) in their wind tunnel experiments, while Iversen, et al.,[16] find maximum turbulence levels above 15% at $x/b \approx 3$ decreasing with distance to 9% at $x/b \approx 8$ ($\Gamma_0/\nu = 1.4 \times 10^5$). Spectra of the velocity fluctuations on the 400 ft rope are given in Figs. 14-16. These figures are typical of spectra analyzed on two different passes through the vortex for each rope length. There were no trends with rope length and, therefore, we have omitted graphs for the 200 and 800 ft ropes.

The lowest spectrum, marked clear air, was taken at a radial distance somewhat greater than $r/c>0.32$ (20 in.) and is primarily instrumentation noise. A noticeable trend in the clear air spectrum is a spike at 100 Hz in the tangential and radial velocity spectra. Recall that our vortex location method was very inaccurate when the vortex was far from the probes, and that a new vortex location was computed every 1/100 s. Consequently, the spectral peaks in the clear air curves seem to be an artifact of noise in the vortex core locating calculation and its inherent error at large radial distances.

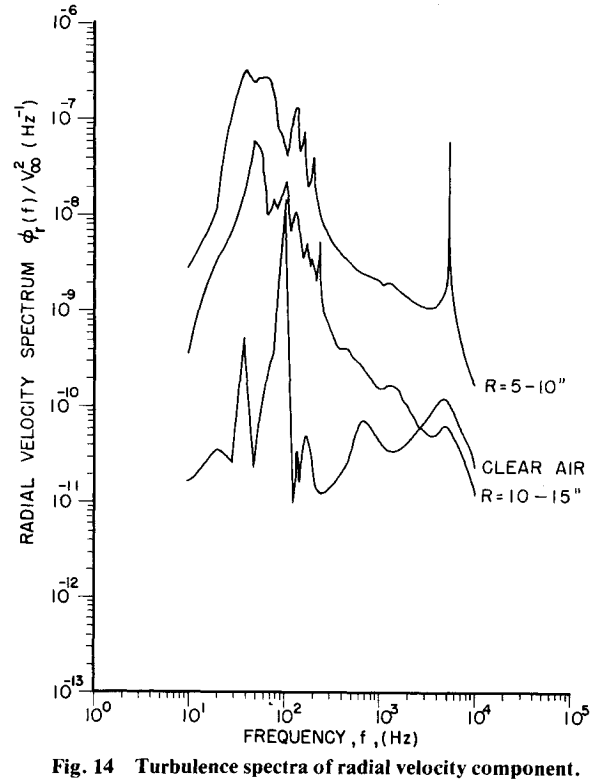

Fig. 14 Turbulence spectra of radial velocity component.

Since the axial component of the velocity does not depend upon the vortex location calculations, there is no corresponding spike at 100 Hz. All spectra increase as one moves toward the vortex core (there were no data within the core), and the spectral level of the different components are roughly the same at similar radial positions.

The low turbulence levels measured are consistent with the low eddy viscosity and corresponding high values for the mean tangential velocity which were discussed earlier. It is interesting to note that there are some sophisticated models of turbulence which also predict the turbulence intensity.[6,8,9,17]

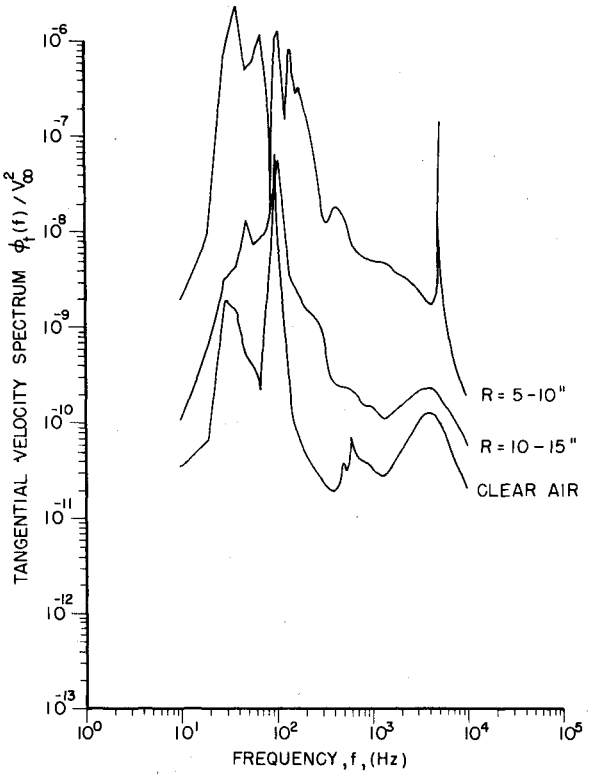

Fig. 15 Turbulence spectra of tangential velocity component.

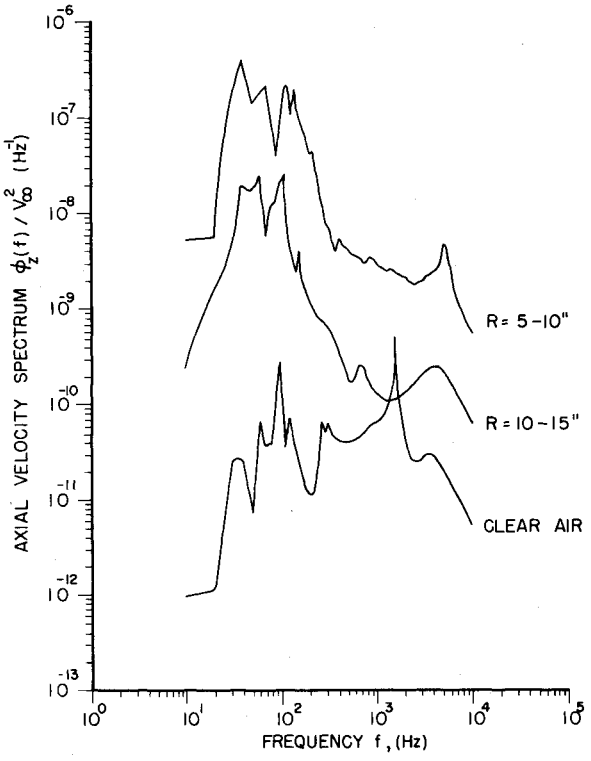

Fig. 16 Turbulence spectra of longitudinal velocity component.

These models use several empirical constants, which are in principle universal and are determined from simpler turbulence experiments. Although many quantitative aspects of these theories are not verified by our results, these theories predict that an initial turbulence distribution should decay and in some cases be completely damped out in the core region.

One additional comment on the influence of the turbulence levels on the velocity profiles should be considered. Our experiment with a rectangular wing and a well-rounded tip were conducted in very smooth air and resulted in large tangential velocities. Corsiglia, et al.,[18] conducted a test which was in a certain sense the opposite of ours as the vortex contained a large amount of turbulence. They placed a rectangular plate on the upper wing surface at the tip so that it was perpendicular to the freestream. The turbulence generated by the plate was inducted into the vortex and resulted in a tangential velocity profile much lower than profiles measured at the same location with the plate removed. Their tests were made at only one downstream location so that a decay rate could not be established. The conclusion is that the initial level of turbulence is very important in the history of the vortex and that, since production of turbulence in a vortex is very small, there may not be a single asymptotic state to which all vortices will eventually decay.

Summary and Conclusions

Flight measurements of the wing tip vortex produced by a DeHavilland Beaver revealed a very small, high velocity vortex with very low turbulence levels. The Lamb vortex equation gave a good fit to the data, and measurements at three downstream locations verified the similarity law by giving a $x^{-1/2}$ decay. Although the decay followed the same law as many previous measurements, the magnitude of the tangential velocity was a factor of 2.5 larger than previous experiments. (The magnitude of Squire's constant was $\nu_t/\Gamma_0 \approx 10^{-5}$.) We attribute the discrepancy between our experiments and previous results to the fact that we had a large-scale wing with a well-rounded tip operating in a very smooth and stable atmosphere. The turbulence introduced into the vortex profile, both initially and from the atmosphere surrounding the vortex, was extremely low. Since the vortex decayed to a different asymptotic state than previous measurements, we conclude that a unique similarity region independent of Γ_0/ν, independent of the initial profile, and independent of the initial turbulence conditions may not exist. The initial turbulence level and vortex formation process may influence the entire vortex decay process. It would appear that past studies have underestimated the importance of the shape of the tip and its influence upon both the initial tangential velocity profile and the initial turbulence in the vortex.

Acknowledgments

Funding for this research was provided by the National Science Foundation under grants GK-41012 and ENG75-16987. The authors would also like to acknowledge the able help provided by J. Spurgeon in designing and constructing the electronics, B. Lynn for flying the sailplane, and R. Wilke and H. Chevalier of Texas A&M for providing and piloting the DeHavilland Beaver.

References

[1] Ciffone, D.L. and Orloff, K.L., "Far Field Wake Vortex Characteristics of Wings," *Journal of Aircraft*, Vol. 12, May 1975, pp. 464-470.

[2] Iversen, J.D., "Inviscid to Turbulent Transition of Trailing Vortices," AIAA Paper 75-883.

[3] De Neufville, A., "The Dying Vortex," *Proceedings of Fifth Midwest Conference on Fluid Mechanics*, University of Michigan, Ann Arbor, 1957, p. 365. (Also see *Laminar Flow Theory*, F.K. Moore, Ed., Princeton University Press, Princeton, N.J., 1964, p. 407.)

[4] Squire, H.B., "The Growth of a Vortex in Turbulent Flow," *Aeronautical Quarterly*, Vol. 16, 1965, pp. 302-306.

[5] Iversen, J.D., "Correlation of Turbulent Trailing Vortex Decay Data," *Journal of Aircraft*, Vol. 13, May 1976, pp. 338-342.

[6] Knight, D.D. and Saffman, P.G., "Turbulence Model Predictions for Flows with Significant Mean Streamline Curvature," Rept. AM77-1 Applied Mathematics, California Institute of Technology, Pasadena, Calif., June 1977.

[7] Soskic, Nikola, "Flight Measurements of the Wing Tip Vortex," Ph.D. dissertation, Mechanical Engineering, The University of Texas, Austin, Dec. 1977.

[8] Donaldson, C. duP., "Calculation of Turbulent Shear Flows for Atmospheric and Vortex Motions," *AIAA Journal*, Vol. 10, Jan. 1972, pp. 4-12.

[9] Saffman, P.G., "Structure of Turbulent Line Vortices," *Physics of Fluids*, Vol. 16, Aug. 1973, pp. 1181-1188.

[10] Nielsen, J.N. and Schwind, R.G., "Decay of a Vortex Pair Behind an Aircraft," *Aircraft Wake Turbulence and Its Detection*, Plenum Press, New York, 1971, pp. 413-454.

[11] Kuhn, G.D. and Nielsen, J.N., "Analytical Studies of Aircraft Trailing Vortices," AIAA Paper 72-42.

[12] Ciffone, D.L., "Correlation for Estimating Vortex Rotational Velocity Downstream Dependence," *Journal of Aircraft*, Vol. 11, Nov. 1974, pp. 716-717.

[13] Chigier, N.A. and Corsiglia, V.R., "Wind Tunnel Studies of Wind Wake Turbulence," *Journal of Aircraft*, Vol. 9, Dec. 1972, pp. 820-825.

[14] Thompson, D.H., "Experimental Study of Axial Flow in Wing Tip Vortices," *Journal of Aircraft*, Vol. 12, Nov. 1975, pp. 910-911.

[15] Singh, P.I. and Uberoi, M.S., "Experiments of Vortex Stability," *Physics of Fluids*, Vol. 19, Dec. 1976, pp. 1858-1863.

[16] Iversen, J.D., Park, S., and Backhus, D.R., "Hot-Wire, Laser Anemometer and Force Balance Measurements in Cross-Sectional Planes of Single and Interacting Vortices," AIAA Paper 78-1194.

[17] Donaldson, C. duP. and Bilanin, A.J., "Vortex Wakes of Conventional Aircraft," AGARDgraph No. 204, May 1975.

[18] Corsiglia, V.R., Schwind, R.G., and Chigier, N.A., "Rapid Scanning, Three-Dimensional Hot-Wire Anemometer Surveys of Wing Tip Vortices," *Journal of Aircraft*, Vol. 10, Dec. 1973, pp. 752-757.